A sub-grid scale closure for nonlinear hillslope sediment transport models

Vamsi Ganti,[1] Paola Passalacqua,[2] and Efi Foufoula-Georgiou[1]

[1]   Hillslope sediment transport models express the sediment flux at a point as a function of some topographic attributes of the system, such as slope, curvature, soil thickness, etc., at that point only (referred here as "local" transport models) or at an appropriately defined vicinity of that point (referred here as "nonlocal" transport models). Typically, topographic attributes are computed from digital elevation data (DEMs) and thus their estimates depend on the DEM resolution (1 m, 10 m, 90 m, etc.) rendering any sediment flux computation scale-dependent. Often calibration compensates for this scale-dependence resulting in effective parameterizations with limited physical meaning. In this paper, we demonstrate the scale-dependence of local nonlinear hillslope sediment flux models and derive a subgrid scale closure via upscaling. We parameterize the subgrid scale closure in terms of the low resolution, resolved topographic attributes of the landscape, thus allowing the reliable computation of a scale-independent sediment flux from low resolution digital elevation data. We also show that the accuracy of the derived subgrid scale closure model depends on the dimensionless erosion rate and the dimensionless relief of any given basin. Finally, we present theoretical arguments and demonstrate that the recently proposed nonlocal sediment flux models are scale-independent. These concepts are demonstrated via an application on a small basin (MR1) of the central Oregon Coast Range using high-resolution lidar topographic data.

1.   Introduction

[2]   The generation and movement of sediment on hillslopes has been the subject of continuous theoretical and field work since the pioneering conceptualizations of *Gilbert* [1877, 1909] and the mathematical formalisms introduced later by *Culling* [1960, 1963, 1965]. *Culling* [1963] proposed that the magnitude of the average rate of downslope sediment flux depends linearly on the magnitude of the local gradient:

$$q_{s,L} = K_L |\nabla z| \qquad (1)$$

where $q_{s,L}$ is the volumetric sediment transport rate per unit contour length, z is local hillslope elevation, $|\nabla z|$ is the magnitude of the local hillslope gradient, and K_L is the proportionality constant (a diffusion-like coefficient) which depends on climate and material. The value of K_L has been

estimated from a variety of approaches including field and experimental tests (e.g., see *Martin and Church* [1997] and *Fernandes and Dietrich* [1997] for reviews) and process-specific derived models [e.g., *Kirkby*, 1971; *Gabet*, 2000; *Furbish et al.*, 2007]. Excellent reviews and further references are provided by *Dietrich et al.* [2003] and *Tucker and Hancock* [2010].

[3]   The linear slope-dependent sediment transport model of equation (1) has been found inadequate to explain the observed sediment flux on steep slopes (slopes in excess of 20%) and nonlinear sediment transport models have been proposed [e.g., *Scheidegger*, 1961; *DePloey and Savat*, 1968; *Kirkby*, 1984; *Andrews and Hanks*, 1985; *Pierce and Colman*, 1986; *Andrews and Bucknam*, 1987; *Anderson and Humphrey*, 1990; *Anderson*, 1994; *Howard*, 1994; *Roering et al.*, 1999; *Gabet*, 2000]. A nonlinear sediment transport model widely used is of the form:

$$q_s = \frac{K|\nabla z|}{1 - (|\nabla z|/S_c)^2} \qquad (2)$$

where q_s is the magnitude of the nonlinear sediment flux, K is a diffusivity, and S_c is the so-called critical gradient. The above equation has been derived from different assumptions and theories and has been verified by field and experimental studies [*Andrews and Bucknam*, 1987;

[1]Department of Civil Engineering, National Center for Earth-surface Dynamics, St. Anthony Falls Laboratory, University of Minnesota, Minneapolis, Minnesota, USA.
[2]Department of Civil, Architectural, and Environmental Engineering, University of Texas at Austin, Texas, USA.

Roering et al., 1999, 2001; *Roering*, 2008]. From equation (2) one observes that at small gradients, the nonlinear flux model imitates linear diffusive transport. However, as local gradients approach a critical threshold gradient (S_c), the nonlinear flux model depicts an accelerated diffusion on hillslopes and the magnitude of the nonlinear sediment flux approaches infinity. The diffusivity and the critical gradient (K and S_c) are calibrated parameters [e.g., *Roering et al.*, 1999; *Heimsath et al.*, 2001]. Both equations (1) and (2) use the magnitude of the local gradient at every pixel to compute the sediment flux at that location. We will call both these transport models as "local", linear and nonlinear, respectively. The local sediment transport models inherently assume the existence of a representative elementary volume (that incorporates the heterogeneities of the landscape) where the model can be applied.

[4] Recently, a new approach has emerged motivated by the observation that the scales of transport or particle displacement on hillslopes span a wide range as a result of very heterogeneous disturbance processes (such as gopher mounds, rain splash, wood blockage, tree throw, etc) [*Foufoula-Georgiou et al.*, 2010; *Furbish and Haff*, 2010]. Thus, there is no separation between the scales of transport and the scale of the system itself, putting in question the standard local gradient theory formulations (e.g., see review by *Foufoula-Georgiou and Passalacqua* [2012]). Nonlocal theories of sediment transport on hillslopes have been proposed using discrete particle-based models [*Tucker and Bradley*, 2010] or a fractional diffusion continuum formulation [*Foufoula-Georgiou et al.*, 2010]. The continuum nonlocal model takes the general form:

$$q_s^{\star}(x) = K^{\star} \int_0^x g(l) \left| \frac{\partial z(x-l)}{\partial x} \right| dl \qquad (3)$$

where $q_s^{\star}$ is the magnitude of the nonlocal flux, $K^{\star}$ is the measure of the diffusivity, $g(l)$ is a weighting function which takes into account the upslope history of the system, and x is the distance from the ridgetop along the hillslope flow path. When the weighting function takes a power law form, $g(l) \sim l^{1-\alpha}$ where $1 < \alpha \leq 2$, then the above equation can be cast into a fractional diffusive flux model for sediment transport on hillslopes [*Foufoula-Georgiou et al.*, 2010]. The nonlocal transport models are inherently scale-free and do not assume the existence of a representative elementary volume.

[5] It has been discussed in the literature that the computation of local gradients and many of the geomorphic and hydrologic quantities (e.g., width function, channel initiation threshold, topographic index, etc.) of a catchment are strongly dependent on the resolution of the digital elevation models (DEMs) used [e.g., *Montgomery and Foufoula-Georgiou*, 1993; *Zhang and Montgomery*, 1994; *Walker and Willgoose*, 1999; *Zhang et al.*, 1999; *Evans and Willgoose*, 2000; *Stark and Stark*, 2001; *Zhang et al.*, 2002; *Dietrich et al.*, 2003; *Boardman*, 2006; *Passalacqua et al.*, 2006; *Sorensen and Seibert*, 2007; *Foufoula-Georgiou et al.*, 2008] and even on the gridding methods used in building the DEM [e.g., *Hancock*, 2005, 2006]. Hence, any local sediment transport model (linear or nonlinear) that is a function of the local gradients will be scale-dependent. For example, using 90 m or 30 m DEMs will

result in different local gradients than those computed from a 1 m DEM. How then is the scale-dependence of gradients to be handled in computing the sediment flux from equations (1) or (2)? One can argue that this can be handled by appropriate calibration of the flux equation to local data to yield an effective (scale-dependent) parameter K [*Anderson*, 1994]. This is unsatisfying in the long-run as this parameter loses its physical meaning. At the same time both equations (1) and (2) physically apply at some scale that is assumed to be the representative elementary control volume for the application of the local sediment transport models (e.g., determined to be the scale which averages over biotic processes [*Roering et al.*, 2010]). For example equation (2) has been derived from ballistic particle transport considerations [*Andrews and Bucknam*, 1987] or from the balance of frictional and gravitational forces at a scale below which topography is dominated by biotic processes [*Roering et al.*, 1999, 2010]. Thus, in principle if equations (1) and (2) were to be applied at length scales greater than the scale of the pre-defined representative elementary volume, new mean field equations would need to be derived via upscaling. These mean field equations would not only involve the same model formulation evaluated at the larger scale, but would also involve additional terms which take into account the variability that lies within the scale of application. The additional terms are called the subgrid scale closure terms as they account for the subgrid variability of the landscape and need to be taken into account while applying flux models at larger scales. In simple words, applying flux models at a larger scale would not simply involve keeping the model equation intact and tuning the parameter K, but it would instead involve the addition of a closure term to incorporate the variability of gradients within the scale of averaging.

[6] The scope of this paper is to put forward in a formal way the scale-dependence of the local, nonlinear sediment flux models (section 2), and to derive the closure term for the nonlinear sediment flux model of equation (2) (section 3). The parameterization and the applicability of the proposed subgrid scale closure model are discussed in sections 4 and 5, respectively. Finally, we present a preliminary analysis that points in the direction that the nonlocal transport model of equation (3) can be scale-independent (section 6). To demonstrate the above concepts we use 2 m lidar topography of a small basin within the Oregon Coast Range. Conclusions and recommendations for further work are given in section 7.

2. Scale-Dependence of Local Nonlinear Transport Models

[7] In this section we demonstrate via an example the scale-dependence of the magnitudes of local gradients and the computed sediment flux using DEMs at different resolutions. We used lidar data from a small watershed (MR1) within the Oregon Coast Range, near Coos Bay, Oregon, collected at a resolution of approximately 2 m (see Figure 1). Details about this site are discussed by *Roering et al.* [1999].

[8] Computation of local gradients and curvatures at different scales requires a "smoothing" and a corresponding "differencing" filtering of the landscapes. The simplest
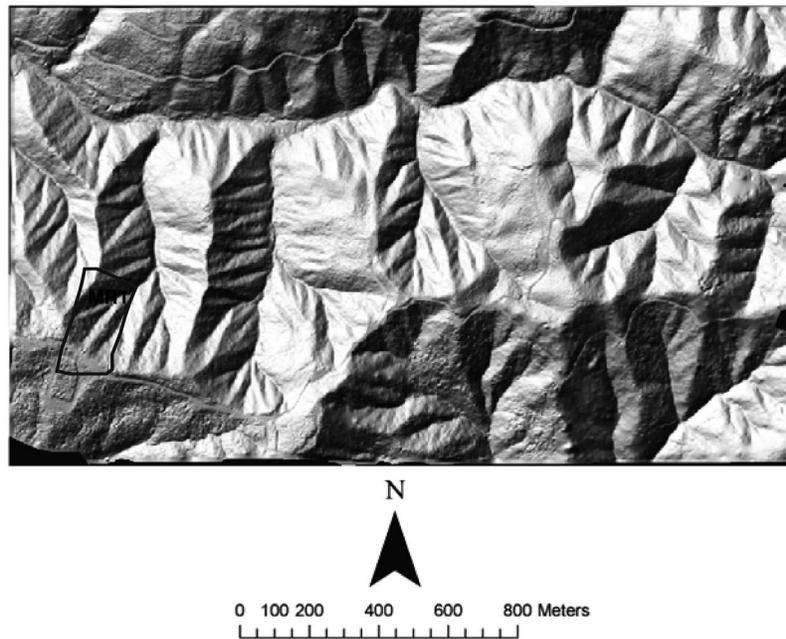
Figure 1. High resolution topographic data of a 2.8 km^2 area in the Oregon Coast Range near Coos Bay, Oregon. The MR1 basin used in this study to demonstrate the scale-dependence of nonlinear hillslope flux model is indicated. The resolution of the data is approximately 2 m.

smoothing filter is the arithmetic averaging in which local gradients and curvatures are the first and second order differences of the smoothed landscape at the corresponding scale. A much more efficient way of implementing both the smoothing and differencing filtering in a single operation is the wavelet-based methodology proposed by *Lashermes et al.* [2007]. A nonlinear filtering framework for smoothing landscapes that enhances the geomorphic features present in the landscape was proposed by *Passalacqua et al.* [2010a] (comparison of the performance of the nonlinear filtering framework and the wavelet-based methodology was shown by *Passalacqua et al.* [2010b]). To be consistent with the upscaling framework used here to derive the subgrid scale closure (section 3), a simple moving averaging of the landscape in boxes of size $\Delta \times \Delta$ m^2 has been used as the smoothing filter and first and second order differencing operations have been performed to compute the local gradients and curvatures at that scale Δ. The results reported here are not sensitive to the choice of the smoothing and differencing filter and similar results were obtained using the wavelet-based methodology.

[9] To evaluate the sediment flux q_s from the hillslope pixels of the study site, one needs to first remove the pixels corresponding to the fluvial or channelized parts of the landscape. For this purpose we use the methodology proposed by *Lashermes et al.* [2007] that is based on the curvature quantile-quantile plot, where any pixel with curvature above a critical threshold value (equal to the curvature value corresponding to the standard normal deviate of 1), which inherently emerges from this quantile plot, corresponds to channelized parts of the landscape (as discussed by *Passalacqua et al.* [2010a] these pixels correspond to the pixels around the centerline of the channels). Figure 2b displays the quantile-quantile plot of the curvatures and

determines the threshold value of 0.1 as the one that delineates hillslope pixels from valleys and channels. Excluding all the pixels for which $\nabla^2 z > 0.1$ yields the pixels of the study site over which the nonlinear hillslope sediment flux model of equation (2) was applied (see Figure 2c). The model parameters used for the computation of the nonlinear sediment flux from the MR1 basin were $K = 0.0032$ m^2/yr and $S_c = 1.25$ [see *Roering et al.*, 1999, Table 1] for calibrated values of the parameters for the Oregon Coast Range). The scales over which the above computations were performed ranged from 2 m (resolution of the data) to 30 m (which is the measure of the length scale of hillslopes obtained from the wavelength corresponding to the scaling break in the power spectral density of lateral elevation transects, taken perpendicular to the trunk stream, of the MR1 basin shown in Figure 2d). For scales larger than 30 m, valley-forming processes dominate the landscape requiring a different transport model.

[10] For the hillslope pixels of the MR1 basin, Figure 3a shows the probability density function (pdf) of the magnitude of the local gradients at different scales Δ. It is observed that the pdfs change with scale not only in shape but also in terms of the mean value $\overline{|\nabla z|}$. Figure 3b shows the numerically evaluated pdf of q_s, $f(q_s)$, using equation (2) on the hillslope pixels of MR1 and for scales $\Delta = 2$, 10 and 30 m. To gain more insight into how the pdf of slopes projects via the nonlinear relationship (2) into the pdf of sediment fluxes q_s we show in Figure 4 a detailed example of the numerical evaluation for $\Delta = 2$ m. It is observed from Figure 4 that the nonlinear shape of the q_s vs $|\nabla z|$ relationship changes the shape of the pdf of $|\nabla z|$ to a more skewed pdf for q_s (since high values of $|\nabla z|$ produce disproportionately large amount of sediment flux). This change of shape of the pdf via the transformation of $|\nabla z|$ to q_s implies that plugging the average
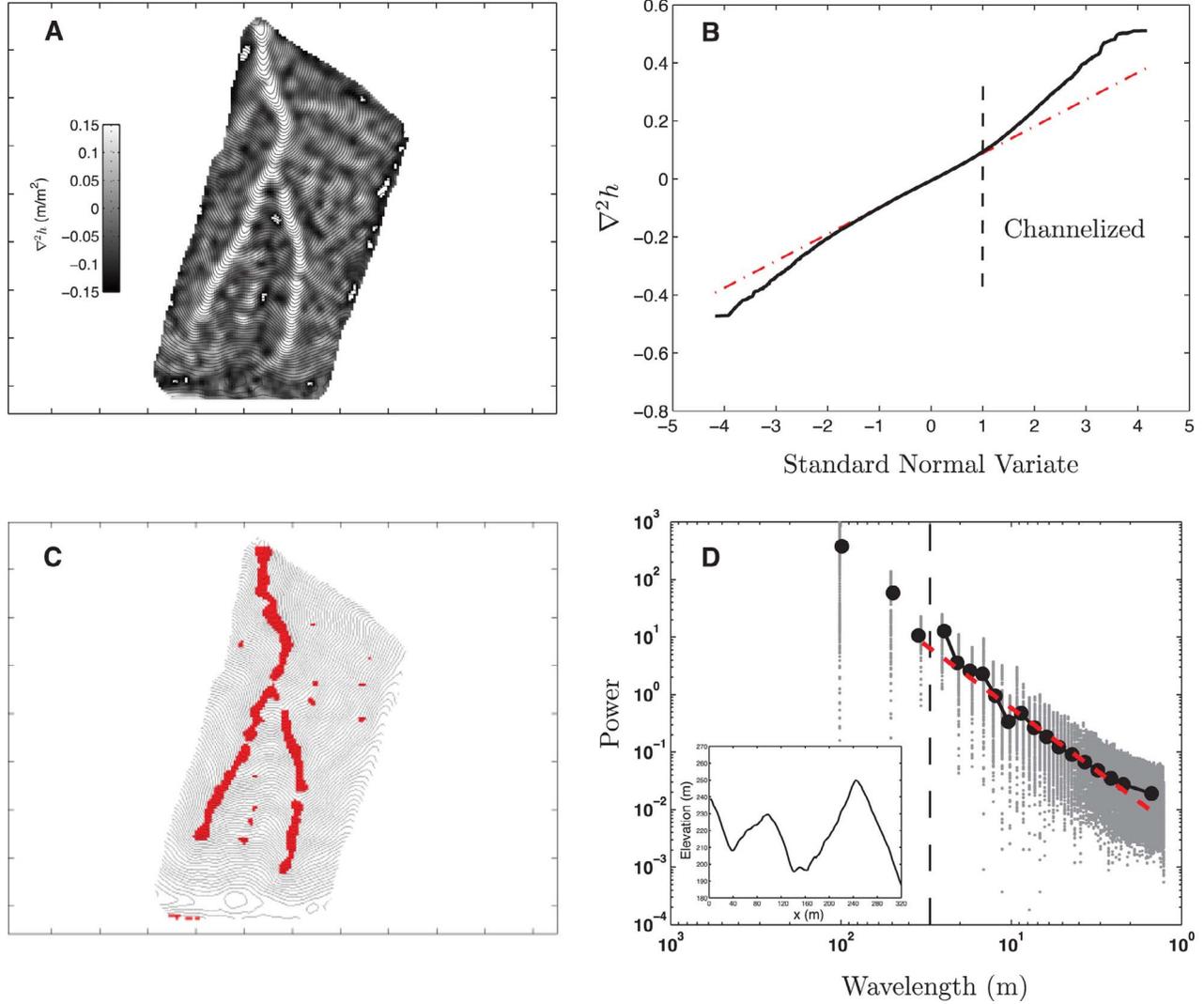
Figure 2. (a) Curvature map of the MR1 basin with the 2 m contour lines overlaid. (b) Quantile-quantile plot of the Laplacian curvatures in the MR1 basin. The deviation of the positive curvature from normality (a straight line in this plot) can be used to identify the channelized pixels as shown by *Lashermes et al.* [2007]. The threshold on curvature for delineating the channelized pixels was found to be ≃0.1. (c) Extracted likely channelized pixels of the MR1 basin (marked in red) using the curvature threshold of 0.1. The computation of the nonlinear hillslope sediment flux was performed on all the pixels of the MR1 basin except for the ones marked in red. (d) Power spectral density of the lateral elevation transects (taken perpendicular to the trunk stream every 2 m) of the MR1 basin. The change in the scaling regime of the power spectral density marks the length scale of hillslopes here considered approximately 30 m as shown with the vertical broken line. The inset plot shows an example elevation transect of the MR1 basin.

local gradient value into equation (2) at a given scale will not result in a good approximation for the average sediment flux at that scale (in fact, it severely underestimates the average sediment flux). This is because the nonlinear relationship in equation (2) implies that $\overline{N(x)} \neq N(\bar{x})$ (where $N(\cdot)$ is some nonlinear function of x), that is:

$$\overline{q_s} = \overline{\frac{K|\nabla z|}{1 - (|\nabla z|/S_c)^2}} \neq \frac{K|\overline{\nabla z}|}{1 - (|\overline{\nabla z}|/S_c)^2} \qquad (4)$$

where the overbar indicates the expected value of the quantity. To get a better approximation of the average flux $\overline{q_s}$ at scale Δ

one needs to consider not only the mean value of the local gradients within a box of size $\Delta \times \Delta$ but also their variability. On the contrary, the average flux $\overline{q}_{s,L}$ for the linear local relationship (1) can be exactly computed by evaluating equation (1) at the box-average slope. This is because for linear relationships: $\overline{L(x)} = L(\bar{x})$. In the next section, we derive the subgrid scale closure for the nonlinear flux model of equation (2).

3. Derivation of Closure for the Local Nonlinear Transport Model

[11] The motivation for deriving the subgrid scale flux for the nonlinear transport model of equation (2) is two-fold.
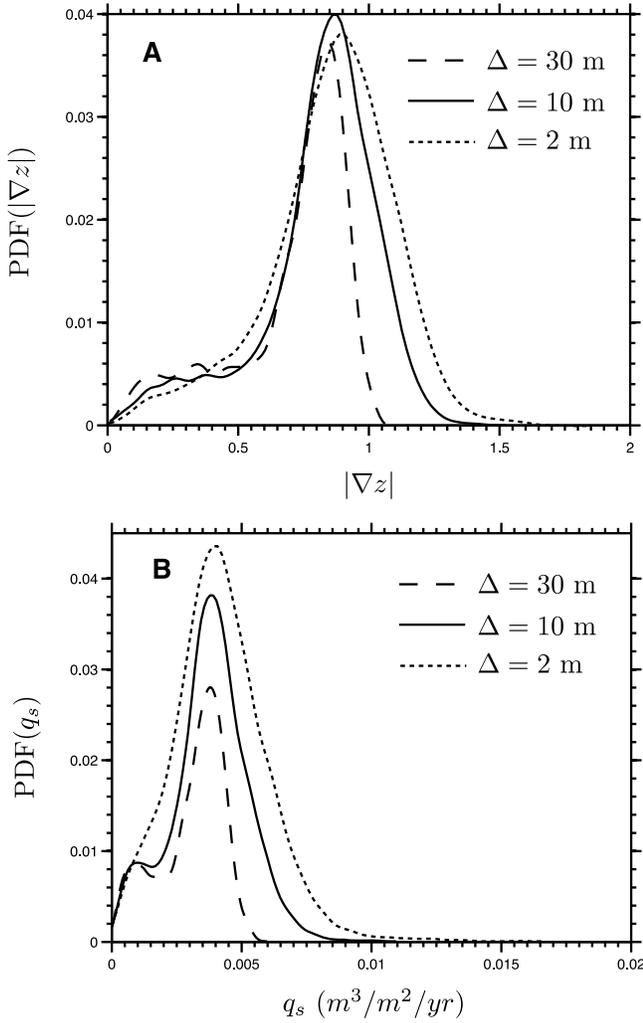
Figure 3. Change of probability density functions of (a) the magnitude of local gradients and (b) the magnitude of the nonlinear sediment flux (equation (2)) with scale Δ computed at the hillslope pixels in the MR1 basin (see Figure 4 for further discussion).

First, DEMs at the resolution of 1 m or 2 m are often unavailable thus forcing the application of the flux models at larger scales. Secondly, even when the high-resolution DEMs are available, the local gradients are computed at scales larger than 1 m to ensure robustness, remove noise, and to average over some stochastic processes such as biotic processes, frost action, etc., that shape the hillslope. Thus, the chosen scale for this computation often introduces unforeseen scale-dependent effects in the computation of sediment flux.
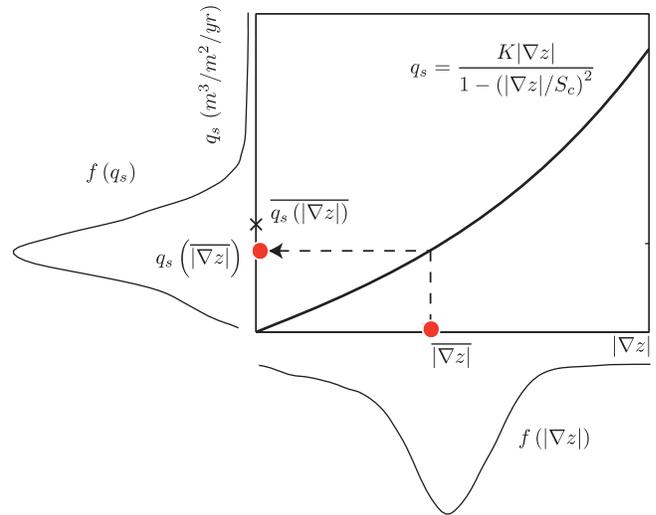
[12] Consider the nonlinear sediment flux model of equation (2). For simplicity of notation, let us denote by S the absolute value of slopes $|\nabla z|$ at the smallest scale, i.e., the scale for which the model of equation (2) is theoretically derived. One can write the nonlinear flux model of equation (2) using Taylor series expansion as:

$$q_s = KS\left(1 + \left(\frac{S}{S_c}\right)^2 + \left(\frac{S}{S_c}\right)^4 + \cdots\right) \quad (5)$$

Since the local slopes are smaller than the critical gradient S_c, the ratio of S to S_c is always less than one and we can neglect the fourth and higher order terms in the series expansion as the contribution to the sediment flux from those terms is negligible (see section 5 for a discussion of the effect of Taylor series approximation on the computed sediment flux). This simplification yields a simple polynomial relation of sediment flux which involves the first and the third powers of the local slope given by:

$$q_s \simeq KS + \frac{K}{S_c^2}S^3 \quad (6)$$

The computed sediment flux using equation (6) from all the hillslope pixels of the MR1 basin shows a strong dependence on scale, as seen from Figure 5 (open circles). The parameters of the nonlinear model used for the computation were $K = 0.0032$ m²/yr and $S_c = 1.25$ [*Roering et al.*, 1999]. Starting with equation (6), which applies at some predefined scale of the representative elementary volume, we derive the subgrid scale closure, i.e., the term that needs to be added to this equation to account for the variability of local slopes within a box of size $\Delta \times \Delta$. We approach this derivation from two different viewpoints: (1) a physical consideration of upscaling the flux to derive a new mean field equation at larger scales, and (2) a statistical viewpoint where upscaling is considered as taking an expectation of the probability distributions of slopes at a given scale.

Figure 4. Using the nonlinear flux model of equation (2), we evaluate how the probability distribution of local slopes $|\nabla z|$ projects into a (derived) probability distribution of sediment flux q_s. We note that the nonlinearity of the functional relationship between $|\nabla z|$ and q_s implies that $\overline{q_s(|\nabla z|)} \neq q_s(|\overline{\nabla z}|)$. That is, computing the flux in a box of size $\Delta \times \Delta$ using the box-average gradient in the nonlinear flux model, $q_s(|\overline{\nabla z}|)$, is not the same as the arithmetic average of the sub-pixel fluxes $\overline{q_s(|\nabla z|)}$. This is due to the nonlinear relationship and the variability of gradients within the box of size $\Delta \times \Delta$. The values of the parameters used here are $K = 0.0032$ m²/yr and $S_c = 1.25$ as reported by *Roering et al.* [1999].
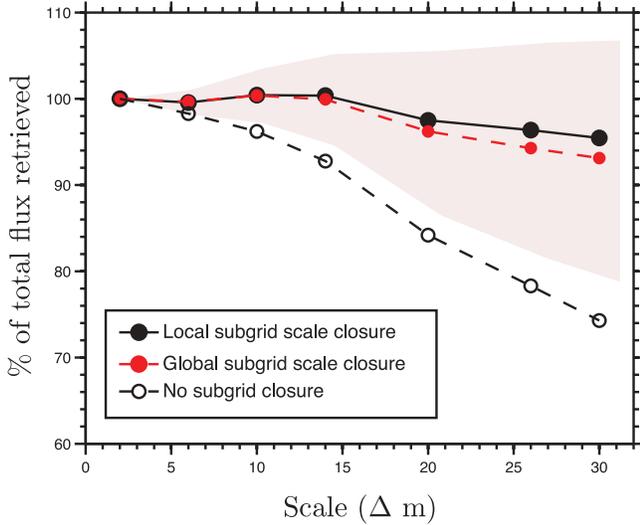
Figure 5. Plot showing the percentage of the total sediment flux computed from the hillslope pixels of MR1 basin that is retrieved at scales larger than $\Delta = 2$ m when compared with the flux computed at scale $\Delta = 2$ m ($\widetilde{q}_{s_\Delta}/q_s$). The open circles denote the sediment flux computed using the nonlinear flux model of equation (6) and the solid circles denote the sediment flux computed using the nonlinear flux model with the proposed second-order closure (equation (10)). The black solid circles indicate the subgrid scale closure term added locally for each box $\Delta \times \Delta$ across the landscape. The solid red circles indicate the flux calculated using the subgrid scale closure parameterized using the global statistics of slope fluctuations across the basin. The shaded area denotes the standard error (evaluated from equation (10) by replacing $Var(S'_\Delta)$ with $std(Var(S'_{\lambda\Delta}))$) in the estimate of the nonlinear flux with the global subgrid scale closure parameterization. The values of the parameters used were $K = 0.0032$ m^2/yr and $S_c = 1.25$ (same as the values calibrated by *Roering et al.* [1999]).

3.1. Subgrid Scale Closure: Physical Viewpoint

[13] Let us denote the upscaled flux at a given scale Δ as $\widetilde{q}_{s_\Delta}$. This flux can be computed by a filtering or upscaling of the right hand side of equation (6) as:

$$\widetilde{q}_{s_\Delta} \simeq \widetilde{KS + \frac{K}{S_c^2}S^3} \qquad (7)$$

At every pixel of the landscape, the magnitude of the gradient, S, can be decomposed into its filtered component at scale Δ, $\widetilde{S}_\Delta$, and its fluctuation around the filtered component, S'_Δ, i.e., $S = \widetilde{S}_\Delta + S'_\Delta$. This operation is akin to the Reynolds decomposition or the Large Eddy Simulation approach used extensively in modeling turbulence [e.g., *Germano et al.*, 1991; *Moin et al.*, 1991; *Meneveau and Katz*, 2000; *Pope*, 2000; *Porté-Agel et al.*, 2000; *Sagaut*, 2002; *Geurts*, 2004; *Pope*, 2004; *Porté-Agel*, 2004; *Passalacqua et al.*, 2006].

[14] Replacing in equation (7) the local slopes, S, by the sum of their filtered components, $\widetilde{S}_\Delta$, and their fluctuations, S'_Δ, and expanding the right hand side results in:

$$\widetilde{q}_{s_\Delta} \simeq K\widetilde{S}_\Delta + \frac{K}{S_c^2}\left(\left(\widetilde{S}_\Delta\right)^3 + \widetilde{S'^3_\Delta} + 3\widetilde{S}_\Delta\widetilde{S'^2_\Delta} + 3\widetilde{S'_\Delta}\left(\widetilde{S}_\Delta\right)^2\right) \quad (8)$$

Noting that $\widetilde{S'_\Delta} = 0$ at any scale Δ (i.e., the average of the fluctuations around the mean is zero), the above equation after rearrangement simplifies to:

$$\widetilde{q}_{s_\Delta} \simeq K\widetilde{S}_\Delta + \frac{K}{S_c^2}\left(\widetilde{S}_\Delta\right)^3 + \frac{K}{S_c^2}\left(3\widetilde{S}_\Delta\widetilde{S'^2_\Delta} + \widetilde{S'^3_\Delta}\right) \qquad (9)$$

By comparing equation (6) with the filtered equation (9), it is observed that they have the same form except for the additional term in the right hand side of equation (9). This term is the so-called subgrid scale closure which needs to be added to the flux model of equation (6) if one uses the filtered slope, $\widetilde{S}_\Delta$, instead of the local slope S in equation (7) to guarantee scale-independence. The terms $\widetilde{S'^2_\Delta}$ and $\widetilde{S'^3_\Delta}$ in the closure represent the second and the third central moments of the slope fluctuations at the given scale Δ. Depending on the statistical nature of the landscape, the contributions of the second-order term (which contains $\widetilde{S'^2_\Delta}$) and the third-order term (which contains $\widetilde{S'^3_\Delta}$) will vary. Our goal is to demonstrate the effect that the variability of the slope fluctuations has on the computed sediment flux at different scales. Thus, we neglect the third order moment in the closure term and approximate the subgrid scale closure term as:

$$\sigma_{sg}(\Delta) \simeq \frac{3K}{S_c^2}\widetilde{S}_\Delta Var(S'_\Delta) \qquad (10)$$

where $\sigma_{sg}(\Delta)$ denotes the subgrid scale flux at a scale Δ, and $Var(S'_\Delta) = \widetilde{S'^2_\Delta}$ denotes the variance of slope fluctuations within a box of size $\Delta \times \Delta$. From a geometrical point of view, smoothing the landscape is equivalent to piecewise linearization of the landscape in boxes of size $\Delta \times \Delta$ m^2 (i.e., fitting a plane to the landscape in boxes of size $\Delta \times \Delta$). The normalized slope fluctuations S'_Δ are a measure of the local curvature of the landscape. Thus, the derived subgrid scale closure, which is dependent on the slope fluctuations at that scale, S'_Δ, accounts for the deviation from the linearization approximation of smoothing (or the deviation of the landscape shape from the fitted plane in boxes of size $\Delta \times \Delta$). The nature of the subgrid scale flux and its parameterization are discussed in section 4. In the next subsection 3.2 we derive the subgrid scale flux from a statistical viewpoint.

3.2. Subgrid Scale Closure: Statistical Viewpoint

[15] Since the upscaling filter using arithmetic averaging is a linear operator, equation (7) can be broken down as:

$$\widetilde{q}_{s_\Delta} \simeq K\widetilde{S}_\Delta + \frac{K}{S_c^2}\widetilde{S^3_\Delta} \qquad (11)$$
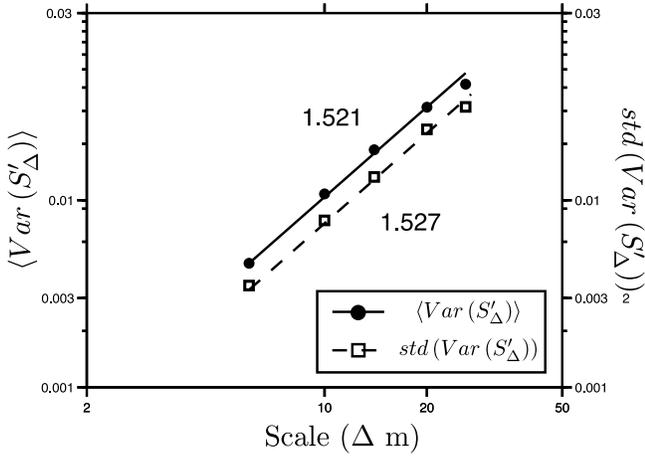
Figure 6. Plot showing the functional dependence of the mean and standard deviation of the variability of slope fluctuations, S'_Δ, on scale Δ in the MR1 basin. The power law dependence on scale of the first two moments of the variance of slope fluctuations within the given scale, ($Var(S'_\Delta)$), allows one to parameterize the subgrid scale closure of equation (10).

i.e., the sum of a linear and a nonlinear term: $q_s = L(S) + N(S)$. The nonlinear term involves the filtering of the third power of S which is not the same as the third power of the filtered term, i.e., $\widetilde{S^3_\Delta} \neq \left(\widetilde{S_\Delta}\right)^3$. The nonlinear term $\widetilde{S^3_\Delta}$ in the right hand side of equation (11) can be written in terms of the slopes at the resolved scale $\widetilde{S}_\Delta$ using the Taylor expansion which is given by:

$$\widetilde{N(S)} = N\left(\widetilde{S}_\Delta\right) + \frac{N''\left(\widetilde{S}_\Delta\right)}{2}Var(S'_\Delta) + \dots$$
$$= \frac{K}{S^2_c}\left(\widetilde{S}_\Delta\right)^3 + \frac{3K}{S^2_c}\widetilde{S}_\Delta Var(S'_\Delta) + \dots \qquad (12)$$

Neglecting the higher order terms in equation (12) and substituting it in equation (11) the subgrid scale closure, which is given by $\sigma_{sg} = \widetilde{N(S)} - N\left(\widetilde{S}\right)$, is the same as that in section 3.1 (equation (10)).

4. Parameterization of the Subgrid Scale Flux

[16] The subgrid scale flux (equation (10)) is dependent on the filtered components of the slopes at the given scale Δ, $\widetilde{S}_\Delta$, the variance of the slope fluctuations S'_Δ within boxes of scale Δ, $Var(S'_\Delta)$, and the parameters of the nonlinear flux model, namely, K and S_c. The filtered components of the slopes, $\widetilde{S}_\Delta$, were computed through a simple moving averaging filter (as detailed in section 2) and the slope fluctuations were then determined by taking the differences of the filtered slopes and the slopes computed at the finest resolution of the landscape. By performing this computation over a range of scales Δ, we gained access to the variance of the slope fluctuations and how this variance changes across the landscape. For a given scale Δ, the subgrid scale variance $Var(S'_\Delta)$ depends on the location of the box of size $\Delta \times \Delta$

within the landscape. When high-resolution data are available, say at a scale of 1 m or 2 m, then the subgrid scale closure term can be computed locally for each box of size $\Delta \times \Delta$ m² by estimating the variance of slope fluctuations within each box ($Var(S'_\Delta)$). The resulting subgrid scale closure, which corrects for the subgrid scale variability of slopes specific to each $\Delta \times \Delta$ box, is referred to here as the local subgrid scale closure. Figure 5 (solid black circles) shows the sediment flux computed using the nonlinear flux model of equation (6) with the proposed locally computed subgrid scale closure. Figure 5 demonstrates that the proposed subgrid scale term alleviates the scale-dependence that the nonlinear flux model suffers from (see open circles in Figure 5). The largest scale to which the computations were performed is equal to the scale of the hillslope, $\Delta = 30$ m (see Figure 2d), as beyond this scale the landscape is shaped by valley-forming processes.

[17] The variance of the slope fluctuations, $Var(S'_\Delta)$, within boxes of size $\Delta \times \Delta$ needed in equation (10) requires data at scales smaller than Δ. In the absence of data at resolution higher than Δ, this quantity is unknown and we need to parameterize it in terms of the resolved quantities of the topographic data at scales larger than Δ (say 2Δ). This can be achieved by investigating the relationship between the variance of slope fluctuations within a given scale and the scale Δ. This parameterization can be done locally (for each pixel of the landscape) or globally for the whole landscape. In global parameterization we use the spatially averaged variance of slope fluctuations over the whole landscape ($\langle Var(S'_\Delta)\rangle$) as a first-order estimate of $Var(S'_\Delta)$ for each pixel at the given scale Δ. The standard error of this estimate for each pixel is quantified by the standard deviation of the variance of slope fluctuations, which quantifies the pixel-to-pixel variability of $Var(S'_\Delta)$ across the landscape. Figure 6 shows the functional dependence of these two quantities ($\langle Var(S'_\Delta)\rangle$ and $std(Var(S'_\Delta))$) on scale for the hillslope pixels of the MR1 basin. A power law relationship was found to provide a very good approximation of the functional dependence of the first two central moments of $Var(S'_\Delta)$ on scale, given by:

$$\langle Var(S'_\Delta)\rangle \sim \Delta^\beta \qquad (13a)$$

$$std(Var(S'_\Delta)) \sim \Delta^\gamma \qquad (13b)$$

where $\langle \cdot \rangle$ denotes the expectation operator and $std(\cdot)$ denotes the standard deviation of the quantity in the parenthesis. This functional dependence provides us with a means of parameterizing the subgrid scale flux in terms of the known quantities of the landscape. For instance, if one were attempting to compute the sediment flux from the nonlinear flux model at a scale Δ, an averaging (or filtering) operation would need to be performed on the DEM to compute the slopes at some larger scale $\lambda\Delta$ ($\lambda > 1$). Then the power law form that has been established in Figure 6 can be invoked to estimate the exponents, β and γ, using:

$$\frac{\langle Var(S'_{\lambda\Delta})\rangle}{\langle Var(S'_\Delta)\rangle} = \lambda^\beta \qquad (14a)$$

$$\frac{std(Var(S'_{\lambda\Delta}))}{std(Var(S'_\Delta))} = \lambda^\gamma \qquad (14b)$$

Once the power law exponents are estimated, the mean and standard deviation of the variance of slope fluctuations at the scale of interest can be extrapolated by using the computed mean and standard deviation of $Var(S'_{\lambda\Delta})$. This operation provides a "global" correction for the computed sediment flux over the whole landscape and thus this subgrid scale term computed using global statistics is referred to here as the "global subgrid scale closure." This can be viewed as informing the flux model with the information about the landscape statistics at higher scales to downscale the variability to an unknown smaller scale. This is a common approach to subgrid scale parameterization in large-eddy simulation [e.g., *Porté-Agel et al.*, 2000] as well as in precipitation [e.g., *Harris and Foufoula-Georgiou*, 2001] and soil moisture [e.g., *Nykanen and Foufoula-Georgiou*, 2001] applications. Practically, the implication of this result is that if one were to have DEM data that is too coarse to get reasonable estimates of the sediment flux (e.g., ASTER or SRTM data), then one can quantify the subgrid scale variance of the slope fluctuations within a given scale using the power law relationships shown in Figure 6 and arrive at a reasonable estimate of the sediment flux by applying the subgrid scale closure correction at each pixel of the landscape.

[18] Figure 5 (solid red circles) shows the computed nonlinear sediment flux with the proposed global subgrid scale correction from all the hillslope pixels of the MR1 basin (using the global average $\langle Var(S'_\Delta)\rangle$ value instead of the box-specific values of $Var(S'_\Delta)$ in equation (10)). The model parameters used were $K = 0.0032$ m^2/yr and $S_c = 1.25$. As seen in Figure 5, the global subgrid-scale correction performs only slightly worse than the local correction model even for scales larger than 20 m. In order to explicitly account for the uncertainty introduced by substituting the local variance of slope fluctuations by their spatially average value, the standard error of estimate was also computed (using the standard deviation of the variance of slope fluctuations available at any scale Δ and the power law relationship established in Figure 6). This standard error of estimate is shown as the shaded area in Figure 5.

5. Applicability of the Subgrid Scale Closure Model

[19] As shown in section 4, the proposed subgrid scale closure model of equation (10), when applied to the MR1 sub basin of the Oregon Coast Range, alleviates much of the scale-dependence that the nonlinear hillslope sediment transport model suffers from. The natural question that arises then is: how general is this result and what attributes of a given landscape control the performance of the proposed subgrid scale closure model? Critical to the derivation of the subgrid scale closure is the Taylor series approximation of equation (2) and its truncation (neglecting the higher order terms in equation (5)). The Taylor series expansion of equation (5) does not capture the steep nonlinearity of the functional form of the nonlinear sediment flux model as the average slope of a hillslope approaches the critical value of S_c ($\overline{S}/S_c \rightarrow 1$) and, therefore, for such values of slopes equation (5) becomes an increasingly less accurate approximation of equation (2) . Thus, this polynomial approximation of the nonlinear sediment transport model would have a direct effect on the performance of the proposed subgrid

scale closure model. In this section, we will explore the applicability of the proposed subgrid scale closure model to real landscapes and highlight the primary physical controls on the accuracy of the proposed model.

[20] Morphologic characteristics of hillslopes (e.g., average slope, hillslope relief) are known to depend on the interplay between tectonic forcings and the climate-dependent erosional processes, and several studies have quantified the dependence of different measures of topographic inclination on denudation rates [see *Roering et al.*, 2007, and references therein]. To study the linkage between the hillslope morphology and denudation, one can combine the nonlinear sediment flux model with the one-dimensional, continuity equation given by:

$$\rho_s \frac{\partial z}{\partial t} = -\rho_s \frac{\partial q_s}{\partial x} + \rho_r U \tag{15}$$

where q_s is the nonlinear sediment flux, U is the rock uplift rate, t is time, x is the horizontal hillslope distance, and ρ_r and ρ_s are densities of rock and soil, respectively. Under the assumption of steady state denudation $\partial z/\partial t \rightarrow 0$ (where the rate of bedrock erosion, E, is equal to the rate of rock uplift, U), *Roering et al.* [2007] derived the one-dimensional, functional forms of the magnitude of local gradient ($S = |\partial z/\partial x|$) and hillslope elevation profiles predicted by the nonlinear sediment flux model in terms of the transport parameters (K and S_c), erosion rate (E), and material properties (ρ_r and ρ_s). Further, they showed that in dimensionless form, the magnitudes of local gradients (S^*) and the hillslope relief (R^*) can be expressed as [*Roering et al.*, 2007]:

$$S^* = \frac{S}{S_c} = \frac{1}{(E^* x^*)}\left(1 - \sqrt{1 + (E^* x^*)^2}\right) \tag{16a}$$

$$R^* = \frac{\overline{S}}{S_c} = \frac{1}{(E^*)}\left(\sqrt{1 + (E^*)^2} - \ln\left(\frac{1}{2}\left(1 + \sqrt{1 + (E^*)^2}\right)\right) - 1\right) \tag{16b}$$

where E^* and x^* are independent dimensionless variables, and $\overline{S}$ is the average slope of the hillslope. The expressions for the dimensionless hillslope distance and dimensionless erosion rate were given by:

$$x^* = \frac{x}{L_H} \tag{17a}$$

$$E^* = \frac{E}{E_R} \tag{17b}$$

where L_H is the hillslope length (measured horizontally from the hilltop to the channel margin) and E_R is a reference erosion rate given by $E_R = KS_c/(2L_H(\rho_r/\rho_s))$. As seen from the above equations, the average slope and dimensionless hillslope relief of a hillslope are primarily controlled by the dimensionless erosion rate, E^*.

[21] To quantify the accuracy of the Taylor series approximation of the nonlinear hillslope sediment flux model, we evaluated the steady state magnitudes of the local gradients predicted by the nonlinear sediment flux model for various values of the dimensionless erosion rates. We then computed
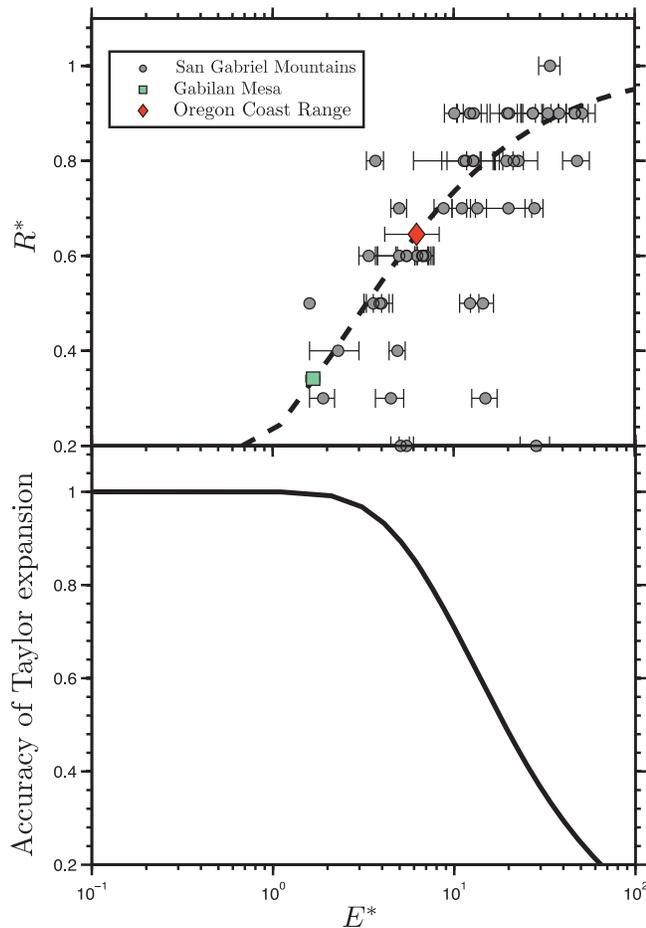
Figure 7. Functional dependence of the accuracy of the Taylor series approximation of the nonlinear sediment flux model on the dimensionless erosion rate, $E*$ (bottom panel). The accuracy of Taylor series approximation is defined as the ratio of the total sediment flux computed from the predicted steady state, equilibrium hillslope profile of the nonlinear sediment transport model using equation (6) to that computed using equation (2). The top panel (broken line) shows the theoretical relationship between the dimensionless relief $R*$ and the dimensionless erosion rate $E*$ derived from the nonlinear sediment flux model of equation (2). Data points from the Oregon Coast Range, the Gabilan Mesa and several catchments from the San Gabriel mountains (as reported by *Roering et al.* [2007] and *DiBiase et al.* [2010]) are also shown on this plot. The above plot can be used to determine whether the proposed closure provides an accurate representation of the subgrid scale fluxes for a given landscape.

the total sediment flux from the hillslope profiles (whose magnitudes of local gradients are given by equation (16a)) using equations (2) and (6). The accuracy of the Taylor series approximation of the nonlinear sediment flux model can then be defined as the ratio of the total flux from the hillslope profile computed using equation (6) to the total sediment flux computed using equation (2). Figure 7 shows the functional dependence of the accuracy of the Taylor series approximation of the nonlinear sediment flux model as a function of the dimensionless erosion rate. The functional dependence of the

dimensionless hillslope relief $R*$ on the dimensionless erosion rate $E*$ is also shown in this plot. As seen in Figure 7, the accuracy of the Taylor series approximation and thus the proposed subgrid scale closure model reduces with an increase in the dimensionless erosion rate. For values of $E* > 10$, the decrease in the accuracy of the Taylor series approximation of the nonlinear sediment flux is significant, as the polynomial approximation of the nonlinear sediment flux model does not capture the threshold behavior of the nonlinear sediment flux model (i.e., the sediment flux does not approach infinity, as the local slope approaches the critical value of S_c). This observation is a manifestation of the fact that hillslope profiles become increasingly planar with an increase in the dimensionless erosion rate and their average slope approaches the critical threshold value ($\overline{S} \rightarrow S_c$). Thus, the ratio of $\overline{S}$ to S_c approaches a value of 1 for higher values of $E*$ (see Figure 7) and the Taylor series approximation (given by equation (6)) does not adequately describe the nonlinear sediment flux model of equation (2). This result has a direct effect on the performance of the proposed subgrid scale closure, as the derivation of the closure is built upon the polynomial approximation of the nonlinear sediment flux model of equation (2).

[22] The reported values of the dimensionless variables for the Oregon Coast Range (of which MR1 is a sub basin) were $E* \sim 6.33$ and $R* \sim 0.64$ [*Roering et al.*, 2007] and thus, from the theoretical relation in Figure 7, we note that the Taylor series approximation provides an adequate representation of the nonlinear sediment flux model of equation (2) for this basin. This results in the good performance of the proposed subgrid scale closure model as shown in section 4. We plotted the dimensionless erosion rates and the dimensionless relief from the Oregon Coast Range, Gabilan Mesa [see *Roering et al.*, 2007, Table 1], and several catchments of the San Gabriel mountains (calculated from Table 1 of *DiBiase et al.* [2010]) in Figure 7. The dimensionless relief for the catchments in San Gabriel mountains were computed (equation (16a)) using the values of average slope ($\overline{S}$) and the magnitude of the critical gradient (S_c) and the dimensionless erosion rates were computed (equation (17b)) using the reported values of the erosion rates (E), K, S_c, L_H, ρ_r and ρ_s used by *DiBiase et al.* [2010, Table 1]. As seen in Figure 7, the Oregon Coast Range, Gabilan Mesa and some catchments of the San Gabriel Mountains have a low dimensionless erosion rate ($E* < 10$), which enables one to apply the proposed subgrid scale closure model to these field sites. We conclude that both the dimensionless erosion rate and the dimensionless hillslope relief are non-parametric measures of the accuracy of the proposed subgrid scale closure and can be used to determine whether the proposed closure provides an accurate representation of the subgrid scale fluxes for a given landscape.

6. Scale-Independence of Nonlocal Flux Model

[23] In this section we put forth the hypothesis that the nonlocal sediment transport model is scale-independent and test this hypothesis using an example computation on a hillslope profile of the MR1 basin. The nonlocal flux model of equation (3) uses a linear combination of slopes along the flow path on the hillslope. Unlike the nonlinear flux model where the flux computation is performed at each pixel of the
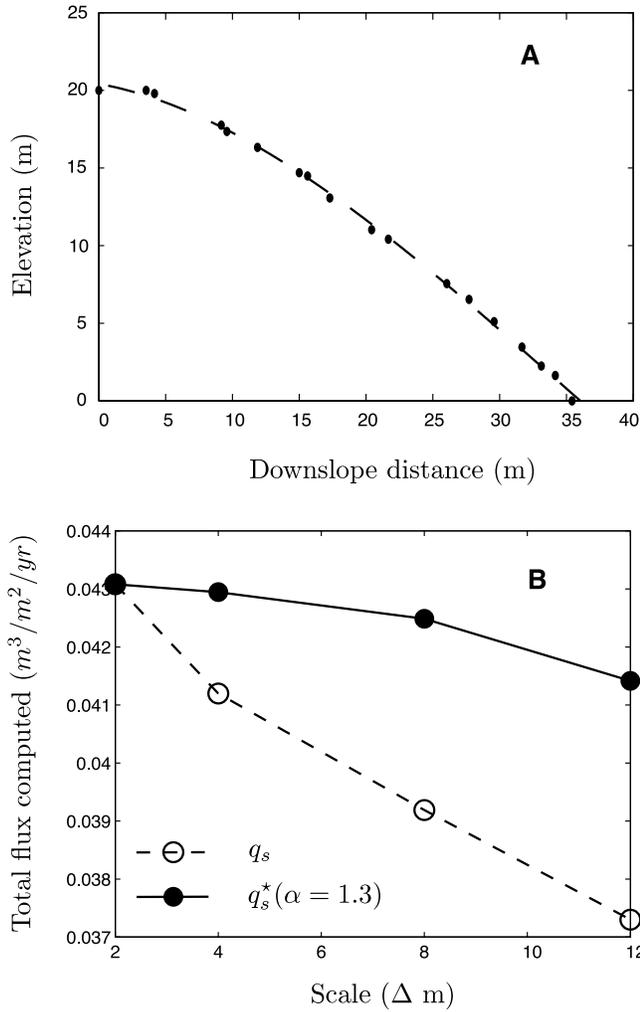
Figure 8. (a) Hillslope profile in the MR1 basin of the Coos Bay region. This profile was reported by *Roering et al.* [1999] and later shown by *Foufoula-Georgiou et al.* [2010] to be consistent with the fractional flux model with the parameter of $\alpha = 1.3$. (b) Flux computed at four different scales along a single profile of the MR1 basin in the Coos bay region. As seen above the nonlinear flux model suffers from scale-dependence of the total flux computed from the hillslope profile, whereas the nonlocal flux model shows very little dependence on scale. The parameters used for the nonlinear flux model were $K = 0.0032$ m²/yr and $S_c = 1.25$. The diffusivity of the fractional flux model, $K^\star$ was calibrated such that the fluxes computed from nonlocal and nonlinear flux models are equal at the smallest scale.

landscape, the nonlocal flux model takes into account the magnitude of local gradients of the upslope topography along the flow path. As shown by *Foufoula-Georgiou et al.* [2010], when the convolution kernel, $g(l)$, in equation (3) takes a power law form the nonlocal flux model can be cast into a fractional derivative form, given by:

$$q_s^\star(x) = K^\star \left| \frac{\partial^{\alpha-1} z}{\partial x^{\alpha-1}} \right| \qquad (18)$$

where $q_s^\star(x)$ is the magnitude of the nonlocal sediment flux, $K^\star$ is a diffusion-like coefficient, $\partial^{\alpha-1}/\partial x^{\alpha-1}$ denotes the fractional derivative operator and x is the distance from the ridgetop along the flow path. The fractional derivative can be computed using the one-shift Grünwald expansion [*Meerschaert and Tadjeran*, 2004]:

$$\frac{\partial^{\alpha-1} z(x)}{\partial x^{\alpha-1}} \simeq \frac{1}{\Delta x^{\alpha-1}} \sum_{k=0}^{N} g_k z(x - k\Delta x + \Delta x) \qquad (19)$$

where g_k are the one-shift Grünwald weights, Δx is the spatial grid size in the numerical evaluation, N is the number of node points upslope of the given point and $\partial^{\alpha-1}/\partial x^{\alpha-1}$ is the fractional differentiation operator of order $\alpha - 1$ ($1 < \alpha \le 2$). The Grünwald weights are given as [*Grünwald*, 1867; *Meerschaert and Tadjeran*, 2004]:

$$g_k = \frac{\Gamma(k - \alpha + 1)}{\Gamma(-\alpha + 1)\Gamma(k + 1)} \qquad (20)$$

where $\Gamma(.)$ is the gamma function. It is readily observed from equations (18) and (19) that computation of the non-local flux, $q_s^\star(x)$, at a location x involves not only the gradient at that location but also gradients upslope of that location. One can write the fractional derivative operator on elevation in equation (18) as a fractional integration on the slopes and thus the nonlocal flux model becomes:

$$q_s^\star(x) = K^\star I_x^{1-\alpha}(S) \qquad (21)$$

where $I_x^{1-\alpha}(\cdot)$ is a fractional integration operation of order $1 - \alpha$ [*Oldham and Spanier*, 1974]. Filtering the above equation yields the following relation:

$$\widetilde{q_{s_\Delta}^\star}(x) = K^\star \widetilde{I_x^{1-\alpha}(S)} \qquad (22)$$

In the above equation, we are performing an averaging of the fractional integral of the slopes, S, which can be decomposed into the sum of their filtered components at a given scale, $\widetilde{S}_\Delta$, and their fluctuations component, S'_Δ. Noting that the fractional integration is a linear operator, the above equation would amount to the sum of the fractional integral of the filtered slope ($\widetilde{S}_\Delta$) and the fractional integral of the average of the fluctuating component of the slopes (S'_Δ). Noting that the latter term is zero ($\widetilde{S'_\Delta} = 0$), equation (22) can be written as:

$$\widetilde{q_{s_\Delta}^\star}(x) = K^\star I_x^{1-\alpha}\left(\widetilde{S}_\Delta\right) \qquad (23)$$

denoting that the filtered flux is equal to the value of the flux calculated by plugging the value of the filtered slope in its original functional form of equation (21). This result demonstrates theoretically that the nonlocal sediment transport model of equation (3) is scale-independent.

[24] We investigate the scale-independence of the nonlocal transport model by computing the sediment flux on a hillslope profile of the MR1 basin at various scales. The hillslope profile chosen was one from the MR1 basin (Figure 8a) that was reported by *Roering et al.* [1999] and later shown by *Foufoula-Georgiou et al.* [2010] to be consistent with the steady state prediction from a nonlocal flux model. Figure 8b shows the total computed sediment flux from this single hillslope profile using both the nonlocal flux model (equation (21)) and the nonlinear flux model (equation (2)).

The parameters of the nonlinear model used were $K = 0.0032$ m^2/yr and $S_c = 1.25$ and $K^\star$ was calibrated such that the total computed sediment flux from the hillslope profile was equal for both the models at the smallest scale (2 m). The value of $\alpha = 1.3$ was chosen, which was estimated from the form of the hillslope profile shown by *Foufoula-Georgiou et al.* [2010]. As shown in Figure 8b, the scale-dependence of the nonlocal flux model is minimal when compared with the nonlinear flux model. This difference, when added up over all the hillslope profiles of the MR1 basin, amounts to considerable scale-dependence in the case of the nonlinear flux model, whereas the negligible scale-dependence of the nonlocal flux model promises to alleviate the issue of scale-dependence when applied to the whole of MR1 sub basin.

[25] The above demonstration was performed on a single hillslope profile only rather than on the whole MR1 basin, as done in section 4. This is because, to the best of our knowledge, the numerical implementation of fractional derivatives on a 2-D field along directed flow paths that possess a tree-like structure is not known. Testing the scale-independence of the nonlocal flux model on a 2-D elevation field is the subject of future research.

7. Conclusions

[26] In this paper, theoretical analysis and high-resolution lidar data were used to demonstrate the scale-dependence of local nonlinear geomorphic transport models of sediment transport on hillslopes. The following conclusions were drawn:

[27] 1. The magnitude of local gradients and consequently the computed sediment flux from a local nonlinear sediment transport model were shown to be strongly dependent on the scale at which the gradients were computed. A simple moving averaging method was used for the purpose of smoothing the 2 m high-resolution lidar data of the MR1 basin in the Oregon Coast Range to create landscapes at lower resolutions. Other smoothing filters have been tested with little difference in the results.

[28] 2. A subgrid scale closure was derived via upscaling of the nonlinear sediment flux model for sediment transport on hillslopes. It is noted that the local nonlinear flux model inherently suffers from scale-dependence owing to the scale-dependent nature of the local gradients and the nonlinear relationship of the sediment flux and local gradients.

[29] 3. The proposed subgrid scale closure that accounts for the variability at scales smaller than the scale Δ at which the model is applied was shown to depend on the model parameters (diffusivity and critical gradient, K and S_c, respectively), the filtered component of the local gradients ($\widetilde{S}_\Delta$), and the variance of the slope fluctuations within the scale Δ ($Var(S'_\Delta)$). The mean and standard deviation of the within-box (of scale Δ) variability of the slope fluctuations were shown to have a power law dependence on scale, thus enabling one to effectively parameterize the unknown variability at a given scale by using statistical information of the landscape from larger scales. It was shown that both the local subgrid scale closure (each box of scale Δ has its own correction derived from its immediate larger-scale neighborhood) and the global subgrid scale closure (same closure for all boxes based on the statistics of the whole landscape)

alleviate the scale-dependence that the nonlinear sediment flux model suffers from.

[30] 4. The accuracy of the proposed subgrid scale model was shown to be directly related to the dimensionless erosion rate (E^*) and the dimensionless hillslope relief (R^*) of a given landscape. It was shown that for large value of the dimensionless erosion rate ($E^* > 10$ and $\overline{S} \rightarrow S_c$) the proposed subgrid scale closure will not perform well as the Taylor series approximation of the nonlinear sediment transport model, on which the proposed subgrid scale closure derivation relies, breaks down.

[31] 5. Finally, the recently proposed nonlocal flux model for sediment transport on hillslopes [*Foufoula-Georgiou et al.*, 2010] was shown theoretically to be scale-independent owing to its inherent scale-free nature and the fact that it does not assume the existence of a representative elementary control volume. It was demonstrated that the nonlocal flux model shows negligible scale-dependence compared to the nonlinear flux model, when applied to a single hillslope profile of the MR1 basin of the Oregon Coast Range.

[32] The conceptual framework for deriving the subgrid scale closure presented in this paper (section 3) is general and can be applied to any nonlinear sediment transport model. The most notable examples in geomorphic transport are the stream power model for bedrock erosion ($\xi \sim A^m S^n$, where ξ is the rate of bedrock erosion, A is the upstream drainage area and S is the local slope) and the bed load sediment transport models ($q_{bl} \sim \tau^a$, where q_{bl} is the bed load sediment flux and τ is the instantaneous shear stress at the bed). The investigation and derivation of the subgrid scale closure models for these nonlinear sediment transport models is a subject of future study.

References

Anderson, R. S. (1994), Evolution of the Santa Cruz Mountains, California, through tectonic growth and geomorphic decay, *J. Geophys. Res.*, *99*(B10), 20,161–20,179.

Anderson, R. S., and N. F. Humphrey (1990), Interaction of weathering and transport processes in the evolution of arid landscapes, in *Quantitative Dynamic Stratigraphy*, edited by T. A. Cross, pp. 349–361, Prentice Hall, Englewood Cliffs, N. J.

Andrews, D. J., and R. C. Bucknam (1987), Fitting degradation of shoreline scarps by a nonlinear diffusion model, *J. Geophys. Res.*, *92*(12), 857–867.

Andrews, D. J., and T. C. Hanks (1985), Scarp degraded by linear diffusion: Inverse solution for age, *J. Geophys. Res.*, *90*(B12), 10,193–10,208.

Boardman, J. (2006), Soil erosion science: Reflections on the limitations of current approaches, *Catena*, *68*, 73–86.

Culling, W. E. H. (1960), Analytical theory of erosion, *J. Geol.*, *68*, 336–344.

Culling, W. E. H. (1963), Soil creep and development of hillside slopes, *J. Geol.*, *71*, 127–161.

Culling, W. E. H. (1965), Theory of erosion on soil-covered slopes, *J. Geol.*, *73*, 230–254.

DePloey, J., and J. Savat (1968), Contribution a létude de lérosion par le splash, *Z. Geomorphol.*, *12*, 174–193.

DiBiase, R. A., K. X. Whipple, A. M. Heimsath, and W. B. Ouimet (2010), Landscape form and millennial erosion rates in the San Gabriel Mountains, CA, *Earth Planet. Sci. Lett.*, *289*, 134–144.

Dietrich, W. E., D. Bellugi, L. S. Sklar, J. D. Stock, A. M. Heimsath, and J. J. Roering (2003), Geomorphic transport laws for predicting landscape form and dynamics, in *Prediction in Geomorphology*, *Geophys. Monogr. Ser.*, vol. 135, edited by P. Wilcock and R. Iverson, pp. 103–132, AGU, Washington, D. C.

Evans, K. G., and G. R. Willgoose (2000), Post-mining landform evolution modelling: 2. Effects of vegetation and surface ripping, *Earth Surf. Processes Landforms*, 25, 803–823.

Fernandes, N. F., and W. E. Dietrich (1997), Hillslope evolution by diffusive processes: The timescale for equilibrium adjustments, *Water Resour. Res.*, 33(6), 1307–1318.

Foufoula-Georgiou, E., and P. Passalacqua (2012), Nonlocal transport theories in geomorphology: Mathematical modeling of broad scales of motion, in *Treatise on Geomorphology*, edited by J. Shroder Jr. and A. Baas, Academic, San Diego, Calif., in press.

Foufoula-Georgiou, E., V. Ganti, P. Passalacqua (2008), Geomorphic transport laws: Non-local flux with classical mass balance, *Res. Rep. UMSI 2008/27*, Univ. of Minn. Supercomput. Inst., Minneapolis.

Foufoula-Georgiou, E., V. Ganti, and W. E. Dietrich (2010), A nonlocal theory of sediment transport on hillslopes, *J. Geophys. Res.*, 115, F00A16, doi:10.1029/2009JF001280.

Furbish, D. J., and P. K. Haff (2010), From divots to swales: Hillslope sediment transport across divers length scales, *J. Geophys. Res.*, 115, F03001, doi:10.1029/2009JF001576.

Furbish, D. J., K. K. Hammer, M. Schmeeckle, M. N. Borosund, and S. M. Mudd (2007), Rain splash of dry sand revealed by high-speed imaging and sticky paper splash targets, *J. Geophys. Res.*, 112, F01001, doi:10.1029/2006JF000498.

Gabet, E. J. (2000), Gopher bioturbation: Field evidence for non-linear hillslope diffusion, *Earth Surf. Processes Landforms*, 25, 1419–1428.

Germano, M., U. Piomelli, P. Moin, and W. H. Cabot (1991), A dynamic subgrid-scale eddy viscosity model, *Phys. Fluids*, 3, 1760–1765.

Geurts, B. J. (2004), *Elements of Direct and Large Eddy Simulations*, 388 pp., R. T. Edwards, Flourtown, Pa.

Gilbert, G. K. (1877), *Report on the Geology of the Henry Mountains*, 160 pp., Govt. Print. Off., Washington, D. C.

Gilbert, G. K. (1909), The convexity of hilltops, *J. Geol.*, 17, 344–350.

Grünwald, A. K. (1867), Uber "begrenzt" derivation und deren anwendung, *Z. Angew. Math. Phys.*, 12, 441–480.

Hancock, G. R. (2005), The use of digital elevation models in the identification and characterization of catchments over different grid scales, *Hydrol. Processes*, 19, 1727–1749.

Hancock, G. R. (2006), The impact of different grid ding methods on catchment geomorphology and soil erosion over long timescales using landscape evolution model, *Earth Surf. Processes Landforms*, 31, 1035–1050.

Harris, D., and E. Foufoula-Georgiou (2001), Subgrid variability and stochastic downscaling of modeled precipitation and its effects on radiative transfer computations, *J. Geophys. Res.*, 106(D10), 10,349–10,362.

Heimsath, A. M., W. E. Dietrich, K. Nishiizumi, and R. C. Finkel (2001), Stochastic processes of soil production and transport: Erosion rates, topographic variation and cosmogenic nuclides in Oregon Coast Range, *Earth Surf. Processes and Landforms*, 26, 531–552.

Howard, A. D. (1994), A detachment-limited model of drainage basin evolution, *Water Resour. Res.*, 30(7), 2261–2285.

Kirkby, M. J. (1971), Hillslope process-response models based on the continuity equation, *Instr. Br. Geogr. Spec. Publ.*, 3, 15–30.

Kirkby, M. J. (1984), Modelling cliff development in South Wales, *Zeitschrift Geomorphol.*, 28 , 405–426.

Lashermes, B., E. Foufoula-Georgiou, and W. E. Dietrich (2007), Channel network extraction from high resolution topography using wavelets, *Geophys. Res. Lett.*, 34, L23S04, doi:10.1029/2007GL031140.

Martin, Y., and M. Church (1997), Diffusion in landscape development models: On the nature of basic transport relations, *Earth Surf. Processes and Landforms*, 22, 273–279.

Meerschaert, M. M., and C. Tadjeran (2004), Finite difference approximations for fractional advection-dispersion flow equations, *J. Comput. Appl. Math.*, 172(1), 65–77.

Meneveau, C., and J. Katz (2000), Scale invariance and turbulence models for large-eddy simulation, *Annu. Rev. Fluid Mech.*, 32, 1–32.

Moin, P., K. D. Squires, and S. Lee (1991), A dynamic subgrid-scale model for compressible turbulence and scalar transport, *Phys. Fluids*, 3, 2746–2757.

Montgomery, D., and E. Foufoula-Georgiou (1993), Channel network source representation for Digital Elevation Models, *Water Resour. Res.*, 29(12), 3925–3934.

Nykanen, D., and E. Foufoula-Georgiou (2001), Soil moisture variability and its effect on scale-dependency of nonlinear parameterizations in coupled land-atmosphere models, *Adv. Water Res.*, 24(9–10), 1143–1157.

Oldham, K. B., and J. Spanier (1974), *The Fractional Calculus*, Academic, New York.

Passalacqua, P., F. Porté-Agel, E. Foufoula-Georgiou, and C. Paola (2006), Application of dynamic subgrid-scale concepts from large-eddy simulation to modeling landscape evolution, *Water Resour. Res.*, 42, W06D11, doi:10.1029/2006WR004879.

Passalacqua, P., T. Do Trung, E. Foufoula-Georgiou, G. Sapiro, and W. E. Dietrich (2010a), A geometric framework for channel network extraction from lidar: Nonlinear diffusion and geodesic paths, *J. Geophys. Res.*, 115, F01002, doi:10.1029/2009JF001254.

Passalacqua, P., P. Tarolli, and E. Foufoula-Georgiou (2010b), Testing space-scale methodologies for automatic geomorphic feature extraction from liar in a complex mountainous landscape, *Water Resour. Res.*, 46, W11535, doi:10.1029/2009WR008812.

Pierce, K. L., and S. M. Colman (1986), Effect of height and orientation (microclimate) on geomorphic degradation rates and processes, late-glacial terrace scarps in central Idaho, *Geol. Soc. Am. Bull.*, 97(7), 869–885.

Pope, S. B. (2000), *Turbulent Flows*, 771pp., Cambridge Univ. Press, New York.

Pope, S. B. (2004), Ten questions concerning the large-eddy simulation of turbulent flows, *New J. Phys.*, 6(35), 1–24, doi:10.1088/1367-2630/6/1/035.

Porté-Agel, F. (2004), A scale-dependent dynamic model for scalar transport in the atmospheric boundary layer, *Boundary Layer Meteorol.*, 112, 81–105.

Porté-Agel, F., C. Meneveau, and M. B. Parlange (2000), A scale-dependent dynamic model for large-eddy simulation: Application to a neutral atmospheric boundary layer, *J. Fluid Mech.*, 415, 261–284.

Roering, J. J. (2008), How well can hillslope evolution models 'explain' topography? Simulating soil production and transport using high-resolution topographic data, *Earth Surf. Processes Landforms*, 33, 2108–2117.

Roering, J. J., J. W. Kirchner, and W. E. Dietrich (1999), Evidence for nonlinear, diffusive sediment transport on hillslopes and implications for landscape morphology, *Water Resour. Res.*, 36(3), 853–870.

Roering, J. J., J. W. Kirchner, and W. E. Dietrich (2001), Hillslope evolution by nonlinear slope-dependent transport: Steady-state morphology and equilibrium adjustment timescales, *J. Geophys. Res.*, 106(B8), 16,499–16,513.

Roering, J. J., J. T. Perron, and J. W. Kirchner (2007), Functional relationships between denudation and hillslope form and relief, *Earth Planet. Sci. Lett.*, 264, 245–258.

Roering, J. J., J. Marshall, A. Booth, M. Mort, and Q. Jin (2010), Evidence for biotic controls on topography and soil production, *Earth Planet. Sci. Lett.*, 298, 183–190.

Sagaut, P. (2002), *Large Eddy Simulation for Incompressible Flows: An Introduction*, 426pp., Springer, New York.

Scheidegger, A. E. (1961), Mathematical models of slope development, *Geol. Soc. Am. Bull.*, 72(1), 37–49.

Sorensen, R., and J. Seibert (2007), Effects of DEM resolution on the calculation of topographical indices: TWI and its components, *J. Hydrol.*, 347, 79–89.

Stark, C. P., and G. J. Stark (2001), A channelization model of landscape evolution, *Am. J. Sci.*, 301, 486–512.

Tucker, G. E., and D. N. Bradley (2010), Trouble with diffusion: Reassessing hillslope erosion laws with a particle-based model, *J. Geophys. Res.*, 115, F00A10, doi:10.1029/2009JF001264.

Tucker, G. E., and G. R. Hancock (2010), Modeling landscape evolution, *Earth Surf. Processes Landforms*, 35, 28–50.

Walker, J. P., and G. R. Willgoose (1999), On the effect of digital elevation model accuracy on hydrology and geomorphology, *Water Resour. Res.*, 35(7), 2259–2268.

Zhang, W., and D. R. Montgomery (1994), Digital elevation model grid size, landscape representation, and hydrologic simulations, *Water Resour. Res.*, 30(4), 1019–1028.

Zhang, X., N. A. Drake, J. Wainwright, and M. Mulligan (1999), Comparison of slope estimates from low resolution dems: Scaling issues and a fractal method for their solution, *Earth Surf. Processes Landforms*, 24, 763–779.

Zhang, X., N. A. Drake, and J. Wainwright (2002), Scaling land surface parameters for global-scale soil erosion estimation, *Water Resour. Res.*, 38(9), 1180, doi:10.1029/2001WR000356.

E. Foufoula-Georgiou and V. Ganti, Department of Civil Engineering, National Center for Earth-surface Dynamics, St. Anthony Falls Laboratory, University of Minnesota, 2 Third Ave. SE, Minneapolis, MN 55414, USA. (efi@umn.edu)

P. Passalacqua, Department of Civil, Architectural, and Environmental Engineering, University of Texas at Austin, 1 University Station C1786, Austin, TX 78712, USA.